High temperature thermoelectric efficiency in $Ba_8Ga_{16}Ge_{30}$

Eric S. Toberer,[1] M. Christensen,[2] B. B. Iversen,[2] and G. Jeffrey Snyder[1,*]
[1]*Materials Science, California Institute of Technology, Pasadena, California 91125, USA*
[2]*Centre for Energy Materials, Department of Chemistry and iNANO, University of Aarhus, Langelandsgade 140, DK-8000 Aarhus C, Denmark*

(Received 6 August 2007; revised manuscript received 8 October 2007; published 20 February 2008)

The high thermoelectric figure of merit (zT) of $Ba_8Ga_{16}Ge_{30}$ makes it one of the best n-type materials for thermoelectric power generation. Here, we describe the synthesis and characterization of a Czochralski pulled single crystal of $Ba_8Ga_{16}Ge_{30}$ and polycrystalline disks. Measurements of the electrical conductivity, Hall effect, specific heat, coefficient of thermal expansion, thermal conductivity, and Seebeck coefficient were performed up to 1173 K and compared with literature results. Dilatometry measurements give a coefficient of thermal expansion of 16×10^{-6} K^{-1} up to 1175 K. The trend in electronic properties with composition is typical of a heavily doped semiconductor. The maximum in the thermoelectric figure of merit is found at 1050 K with a value of 0.8. The correction of zT due to thermal expansion is not significant compared to the measurement uncertainties involved. Comparing the thermoelectric efficiency of segmented materials, the effect of compatibility makes $Ba_8Ga_{16}Ge_{30}$ more efficient than the higher zT n-type materials SiGe or skutterudite $CoSb_3$.

DOI: 10.1103/PhysRevB.77.075203 PACS number(s): 84.60.Rb, 72.20.Pa

INTRODUCTION

Thermoelectric materials are of great interest due to their ability to use waste heat to generate electricity and as solid state Peltier coolers. Currently, widespread utilization of thermoelectric devices is limited by the low efficiency of the constituent materials. The maximum thermoelectric material efficiency is determined by the dimensionless figure of merit zT ($\alpha^2\sigma T/\kappa$), where α is the Seebeck coefficient ($\Delta V/\Delta T$), σ is the electrical conductivity, T is the absolute temperature, and κ is the thermal conductivity. Generally, high zT is difficult to achieve because of the conflicting material properties required.[1,2] The primary conflict has been summarized as the need for the material to be both a phonon glass and an electron crystal. Recent efforts to spatially separate these functionalities into distinct substructures have been successful in a variety of materials [Zn_4Sb_3,[3] Na_xCoO_2,[4] $Yb_{1-x}CaZn_2Sb_2$,[5] and $CeCo_3FeSb_{12}$ (Ref. 6)]. Clathrates, a class of compounds which contain zero-dimensional cages filled with rattling atoms, are one example of this substructure approach (Fig. 1).

The identification of the clathrate $Sr_8Ga_{16}Ge_{30}$ by Nolas *et al.* as a potential high-zT thermoelectric material greatly increased the interest in the transport properties of this class of compounds.[7] This early work estimated a maximum zT in excess of 1.0 above 700 K, which would rival the state of the art PbTe and skutterudite materials.[2] Since then, a variety of clathrate compounds of type $A^{II}_8B^{III}_xB^{IV}_{46-x}$ (A^{II}=Eu, Sr, Ba, B^{III}=group 13 element, and B^{IV}=group 14 element) have been investigated.[8,9] One of the most promising is the clathrate $Ba_8Ga_xGe_{46-x}$, which has estimated maximum zT values ranging from 0.7 to 1.5 for n-type single-crystal samples with nominal x values of 15 to 16.[10–12] The electrical properties of $Ba_8Ga_xGe_{46-x}$ may be tuned by adjusting the Ga-Ge ratio. The carrier concentration reaches a minimum near $x=16$; off this stoichiometry, valence balance leads to n-type (Ge-rich) and p-type (Ga-rich) materials.[13,14]

The highest reported zT for $Ba_8Ga_xGe_{46-x}$ comes from Saramat *et al.*[12] who pulled a large single crystal of $Ba_8Ga_xGe_{46-x}$ which had regions which appear to have an optimum Ga/Ge stoichiometry near $x=15.3$. A peak zT of 1.35 was obtained at 900 K and an extrapolated maximum of 1.63 was predicted at 1100 K. Such a high zT makes the clathrate type I compounds among the most promising materials for thermoelectrics applications.

The lattice thermal conductivity ($\sim$1 W/mK at room temperature) in single-crystalline clathrates[7,14,15] is comparable to that of a glass. Such remarkably low thermal conductivity arises from the host-guest nature of the clathrate structure, shown in Fig. 1, where covalently bound group 13 and 14 elements form host cages in which alkali or alkali earth elements reside. These guest atoms act as phonon scattering centers through rattling processes (described in greater detail below).[8,16,17]

Here, we describe the transport properties of a pulled single crystal of $Ba_8Ga_{16}Ge_{30}$ [shown in Fig. 1(a)] and its polycrystalline analog. The effect of coefficient of thermal expansion is typically ignored but often cited as a source of error. Here, we measure the coefficient of thermal expansion and derive its effect on zT and show it does not significantly alter zT. The measured transport properties are used to calculate zT and compatibility factor (s). Using these values, a model for a segmented thermoelectric is developed and used to predict an overall device efficiency for several different leg structures. We find that the similar zT profile and thermoelectric compatibility factors of $Ba_8Ga_{16}Ge_{30}$ and $CoSb_3$ lead to similar efficiencies at lower temperatures, but the higher stability temperature of the clathrate (1173 K, compared to 923 K for $CoSb_3$) permits application across a larger temperature range, leading to greater overall efficiency.

EXPERIMENTAL METHODS

Crystal growth

Polycrystalline samples were formed from pure elements of barium (99.2%), gallium (99.999%), and germanium

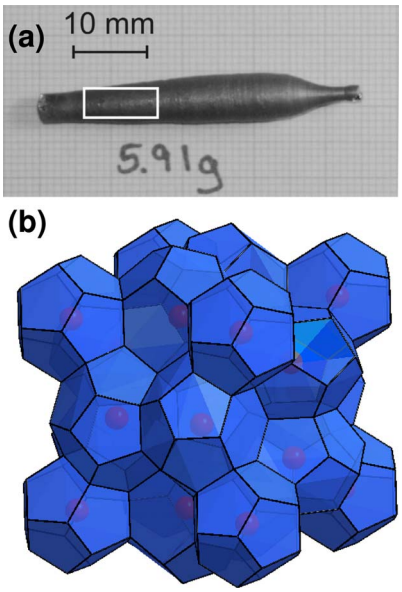

FIG. 1. (Color online) (a) Using the Czochralski pulling method, a large $Ba_8Ga_{16}Ge_{30}$ single crystal was formed. (b) $Ba_8Ga_{16}Ge_{30}$ is a type I clathrate, a structure composed of covalently bound Ga-Ge with cages containing rattling cations. The anion framework of tetrakaidecahedral and dodecahedral polyhedra is shown in blue with red cations.

(99.999%) with a relative stoichiometry of 8:16:29.5. The elements were combined in a glassy carbon crucible, placed in a steel autoclave under argon, and heated to 1325 K in a tube furnace for 4 h. The resulting product was washed with HCl for 24 h to remove impurities. Powder x-ray diffraction of the resulting polycrystalline material revealed no phases other than $Ba_8Ga_{16}Ge_{30}$.

A single-crystal sample was prepared using the Czochralski pulling method. A melt was formed from the polycrystalline material described above in a glassy carbon crucible in an induction furnace. The chamber was filled with He to a pressure of ~6 atm. The crystal was pulled using a seed $Ba_8Ga_{16}Ge_{30}$ single crystal formed previously through the Czochralski method. Pulling the crystal at 10 mm/h resulted in a 5.91 g rod, 4 cm in length. A slow cut diamond saw was used to prepare disks 1–2 mm in thickness from the bottom of this rod.

Characterization

Dilatometry measurements were conducted on a Netzsch 402 from room temperature up to 1173 K. A LEO 1550VP field emission scanning electron microscopy equiped with an Oxford INCA energy 300 x-ray energy dispersive spectrometer (EDS) was used to assess sample homogeneity and composition. Electrical conductivity data (σ) was obtained up to 1173 K using the van der Pauw technique with a current of 100 mA.[18] The Hall coefficient (R_H) was measured on the same apparatus using a magnetic field of 1 T applied sequentially in each direction. From the Hall coefficient, a carrier density (n) was calculated assuming a scattering factor of 1.0 in a single carrier scheme $\left(n=\frac{1}{R_H e}\right)$. The mobility ($\mu$) was calculated according to $\mu=\sigma/(ne)$.

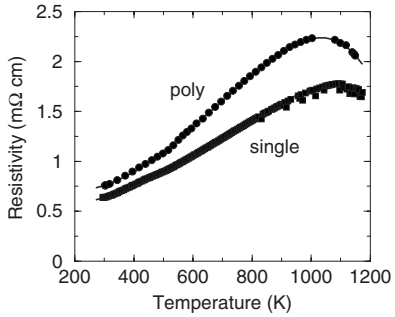

FIG. 2. Resistivity of polycrystalline and single-crystalline $Ba_8Ga_{16}Ge_{30}$. The resistivity behavior is that of a heavily doped semiconductor, with a linear increase in resistivity with temperature until high enough temperatures are reached to increase the carrier concentration by exciting intrinsic carriers.

The Seebeck coefficient was measured up to 1173 K using a temperature gradient created by two pulsing light sources.[19] The temperature was measured with W/Nb thermocouples. The Nb legs of these thermocouples was used to measure the voltage across the sample, from which the absolute Nb voltage was subtracted.[20] In this manner, a ΔT was generated from −5 to 5 K and the slope of the voltage versus ΔT used to calculate the Seebeck coefficient.

Thermal diffusivity of a polycrystalline sample was measured on a Netzsch 457 using a laser flash technique up to 1173 K. The heat capacity was measured in comparison to a Pyroceram 8606 standard. The thermal conductivity (κ) was calculated from the experimental density, diffusivity values, heat capacity, and coefficient of thermal expansion, as described below. As the single crystalline sample was too small for flash diffusivity measurements, the κ obtained for the polycrystalline sample was used in conjunction with the Wiedemann-Franz law to calculate the thermal conductivity of the single crystalline material, as described below.

RESULTS AND DISCUSSION

Property measurements

Dilatometry measurements of a large rod of $Ba_8Ga_{16}Ge_{30}$ single crystal were conducted from room temperature up to 1175 K. A coefficient of thermal expansion of 16×10^{-6} K^{-1} was found across this temperature range. This value is significantly larger than that obtained from prior diffraction studies at low temperatures, 6.4×10^{-6} K^{-1} in the temperature range of 10–300 K for a powder sample[21] and 9×10^{-6} K^{-1} for a single crystal sample up to 400 K.[22]

The $Ba_8Ga_xGe_{46-x}$ samples were found to be homogeneous by EDS, with $x=14\pm1$. As x decreases from 16, $Ba_8Ga_xGe_{46-x}$ is known to become increasingly conductive. Figure 2 shows the electrical resistivity obtained from a slice of the Czochralski pulled $Ba_8Ga_{16}Ge_{30}$ sample. The coefficient of thermal expansion obtained from the dilatometry measurements was used to correct for the changing sample thickness with temperature. The sample is a heavily doped semiconductor, with resistivity increasing with temperature until a peak at 1100 K associated with conduction by intrin-

TABLE I. Summary of electrical resistivity (mΩ cm) and Seebeck coefficient (μV/K) values obtained from various groups. Power factor ($\alpha^2\sigma$) is also calculated (μW/cm K^2). The work by Anno *et al.* is for a range of compositions of $Ba_8Ga_xGe_{40-x}$.

	Reported $Ba_8Ga_{16}Ge_{30}$ properties							
	Single crystal				Polycrystalline			
						Anno *et al.*[d]		
	Present work	Bertini *et al.*[a]	Kuznetsov *et al.*[b]	Saramat *et al.*[c]	Present work	$x=14$	$x=15$	$x=16$
Resistivity								
300 K	0.64	0.65	0.6	0.6	0.8	0.8	1.5	3.1
900 K	1.46	1.8	1.5	1.6	2.0	1.3	3.2	6.6
Seebeck								
300 K	−45	−50	−66	−50	−50	−40	−60	−85
900 K	−135	−180	−170	−180	−135	−120	−260	−280
Power factor								
900 K	13	18	19	20	9	11	21	12

[a]Reference 10.
[b]Reference 11.
[c]Reference 12.
[d]Reference 13.

sic carriers. The resistivity was found to be similar parallel and perpendicular to the growth direction and repeated measurements up to high temperature showed no change in conduction behavior. In comparison to other studies of single crystals of $Ba_8Ga_{16}Ge_{30}$, this single crystalline sample is slightly less resistive (Table I). Figure 2 also shows the electrical resistivity of the polycrystalline sample, which displays a similar, but more resistive, trend with temperature. Table I also summarizes the work by Anno *et al.* on polycrystalline $Ba_8Ga_xGe_{40-x}$ samples,[13] with decreasing x values clearly leading to more conductive materials. Hall effect measurements at rom temperature on the single crystal studied here yield a mobility of 8 cm^2/V s and carrier concentration of 1.2×10^{21} cm^{-3} which corresponds to $x=14.5$.

The Seebeck coefficients of the $Ba_8Ga_{16}Ge_{30}$ single crystal and polycrystalline samples are remarkably similar in these materials (Fig. 3) but lower than the values of the high zT samples (Table I uses 900 K data to include other values from the literature). For semiconductors with mobility independent of carrier concentration, the Seebeck coefficient should decrease with $\ln(\sigma)$, as demonstrated by Rowe and Min for a number of thermoelectric materials.[23] This relationship predicts a slope of k/e (86 μV/K), which is shown with the data from Table I in Fig. 4. Even for degenerate semiconductors and metals, monotonic variation of the Seebeck coefficient with carrier concentration is expected. Plotted in this manner, it is clear that the measured Seebeck coefficients of our materials are lower than one would expect from their electrical conductivities and Ga/Ge ratios. We attribute the departure from the trend to be primarily due to uncertainty in the measurement, and secondarily due to sample variations (e.g., the effect of grain boundaries, impurities, and Ba concentration).

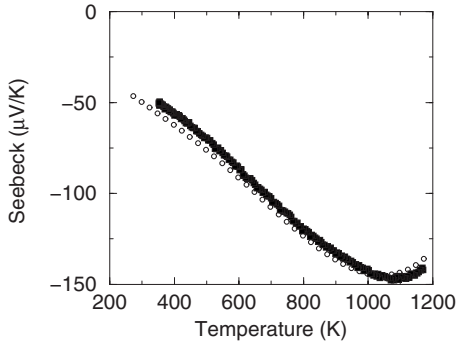

FIG. 3. The Seebeck coefficient ($\Delta V/\Delta T$) rises to −145 μV/K at 1050 K, and then rolls over with increasing intrinsic conduction at higher temperatures. Single crystalline (closed squares) and polycrystalline (open circles) samples show nearly identical behavior.

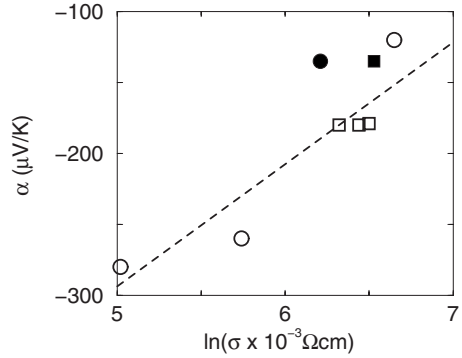

FIG. 4. The natural logarithm of the conductivity and the Seebeck coefficient are linearly related in a semiconductor with a slope of 86 μV/K (shown with dotted line). Prior measurements at 900 K of n-type single crystalline (empty squares) and polycrystalline (empty circles) $Ba_8Ga_xGe_{46-x}$ are shown alongside our single crystalline (filled square) and polycrystalline (filled circle) measurements.

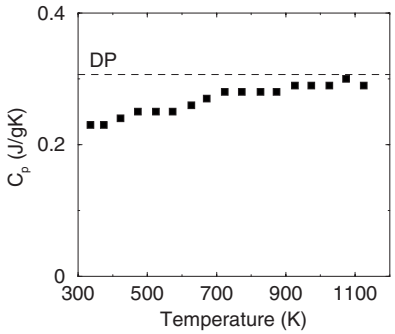

FIG. 5. Heat capacity (C_p) values derived from thermal conductivity measurements of $Ba_8Ga_{16}Ge_{30}$. The C_v value predicted by Dulong and Petit is shown as a dotted line.

The band gap in $Ba_8Ga_{16}Ge_{30}$ may be estimated as ~0.3 eV from the peak in the Seebeck coefficient (−150 μV/K at 1050 K) using the method of Goldsmid and Sharp ($E_g = 2e\sigma_{max}T_{max}$).[24] The band gap for $Ba_8Ga_{16}Ge_{30}$ has previously been estimated theoretically as 0.6–0.9 eV.[25] The effective mass may be obtained from Eq. (1), using the approximation for degenerate semiconductors with the charge carrier scattering distance independent of energy.[26] From the carrier concentration (1.2×10^{21} cm^{-3}) and slope of the Seebeck coefficient (0.156 μV/K^2), the effective mass (m^*) is determined to be ~2.6.

$$\alpha = \frac{8\pi^2 k_B^2}{3eh^2} m^* T \left(\frac{\pi}{3n}\right)^{2/3}. \tag{1}$$

Thermal diffusivity measurements were obtained using a flash diffusivity system on the polycrystalline sample up to 1173 K [Eq. (2)]. The heat capacity can also be determined from the diffusivity experiment by comparing the intensity of the signal with that of a known heat capacity standard, in this case Pyroceram.

At high temperatures the model of Dulong and Petit is typically a good estimate of the specific heat at constant volume C_v, which for $Ba_8Ga_{16}Ge_{30}$ is 0.3065 J/g K. The specific heat at constant pressure C_p is always greater than C_v from thermodynamics. The difference between C_p and C_v increases linearly with temperature for material with constant thermal expansivity and compressibility. Combined, these effects give C_p that crosses the Dulong-Petit value above the Debye temperature and increases linearly thereafter, as seen in SiGe alloys.[27] In this work, the room temperature heat capacity of 0.23 J/g K is somewhat lower than prior room temperature measurements and rises appreciably with the expected linear slope (Fig. 5). Because the measured C_p is less than the value of Dulong and Petit above the Debye temp [about 300 K in $Ba_8Ga_{16}Ge_{30}$ (Ref. 8)], the experimentally determined heat capacity in the high zT region is likely an underestimation but consistent with those previously used. To our knowledge, no high temperature values of heat capacity have been reported in the literature (above 300 K).[28] Prior work has instead employed several approaches to estimate high temperature thermal conductivity in the absence of high temperature C_p: constant values of (a) the room temperature C_p of approximately 0.25–0.29 J/g K,[8,14,29,30] (b) the room temperature value of lattice thermal conductivity and the Wiedemann-Franz law is used to estimate the total thermal conductivity,[11] or (c) the room temperature value of thermal conductivity.[13]

$$\kappa = dDC_p. \tag{2}$$

Thermal conductivity (κ) requires measurement of the thermal diffusivity (D), heat capacity (C_p), and density (d), all values which depend on either the thickness or volume of the sample (values corrected for thermal expansion denoted with a prime). Here, we expand these polynomials to the lowest order in $\Delta l/l$,

$$\frac{d'}{d} = \left(1 - \frac{\Delta l}{l}\right)^3 \cong \left(1 - 3\frac{\Delta l}{l}\right). \tag{3}$$

Diffusivity is a function of the thickness l and half time rise $t_{1/2}$ ($D \approx l^2/t_{1/2}$),

$$\frac{D'}{D} \cong \frac{l'^2}{l^2} = \left(1 + \frac{\Delta l}{l}\right)^2 \cong \left(1 + 2\frac{\Delta l}{l}\right). \tag{4}$$

In a diffusivity measurement in which the sample is illuminated with a calibrated heat flux, the specific heat from the measured temperature rise is proportional to $1/dl$, Eq. (3) is employed along with a correction for the increasing thickness.

$$\frac{d'}{d}\frac{l'}{l} = \frac{1}{\left(1 + \frac{\Delta l}{l}\right)^3}\left(1 + \frac{\Delta l}{l}\right) = \left(1 + \frac{\Delta l}{l}\right)^{-2}. \tag{5}$$

Thus, the specific heat scales as

$$\frac{C_p'}{C_p} \cong \left(1 + 2\frac{\Delta l}{l}\right). \tag{6}$$

Combining Eqs. (3), (4), and (6) in Eq. (2) yields the correction to the thermal conductivity [Eq. (7)], which scales directly with the coefficient of thermal expansion. At the highest temperatures we consider here, this leads to a increase in κ by 1.2%.

$$\frac{\kappa'}{\kappa} \cong \left(1 - 3\frac{\Delta l}{l}\right)\left(1 + 2\frac{\Delta l}{l}\right)\left(1 + 2\frac{\Delta l}{l}\right) \cong \left(1 + \frac{\Delta l}{l}\right). \tag{7}$$

Compared to the errors associated with high temperature property measurements, discussed below, the correction due to the coefficient of thermal expansion in $Ba_8Ga_{16}Ge_{30}$ is less than the known inaccuracies in thermal conductivity measurements.

The electronic and lattice components of the thermal conductivity may be approximated ($\kappa = \kappa_l + \kappa_e$) using the Wiedemann-Franz law (where L is the Lorenz factor, 2.44×10^{-8} J^2/K^2 C^2 for free electrons),

$$\kappa_e = L\sigma T. \tag{8}$$

Figure 6 shows the thermal conductivity dropping (up to 900 K); in accordance with work by Saramat *et al.* and is attributed to phonon-electron and phonon-phonon scattering.[12] Above 1000 K, the thermal conductivity rises due to

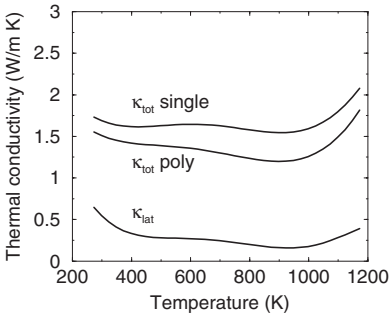

FIG. 6. The total thermal conductivity of polycrystalline and single crystalline $Ba_8Ga_{16}Ge_{30}$ is shown with temperature. The lattice component of the thermal conductivity is extremely low (comparable to a glass) and is derived from the Wiedemann-Franz law.

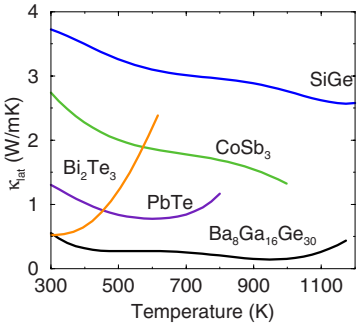

FIG. 7. (Color online) The lattice component of the thermal conductivity of several *n*-type high efficiency thermoelectric materials, including $Ba_8Ga_{16}Ge_{30}$. Values derived from the Wiedemann-Franz law.

the onset of mixed conduction (holes as well as electrons). To the extent that the electrical conductivity increases, the calculated κ_e will also increase. However, mixed conduction adds additional thermal conductivity due to the charge carriers transporting their ionization energy,[31] which is not included in the Wiedemann-Franz law, leading to an increase in the remaining κ_l term (Fig. 6). The lattice thermal conductivity should be nearly identical among all $Ba_8Ga_{16}Ge_{30}$ samples, permitting an estimation of the total thermal conductivity of the single crystal using κ_l of the polycrystalline samples and and the electrical conductivity of the single crystal [employing the Wiedemann-Franz law, Eq. (8)]. An investigation of lattice thermal conductivity in $Ba_8Al_{16}Ge_{30}$ has revealed, however, that synthesis technique can affect the anion framework and the resulting phonon scattering.[32] Figure 6 shows this calculated κ_{tot} for the single crystal sample, which is larger than the polycrystalline sample due to the increased electrical conductivity. The extremely low κ_l observed here, 0.14 W/mK at 1000 K, is approximately κ_{min}.[7] The high zT material formed by Saramat *et al.* is measured to have an even lower κ_l. Similarly, low κ_l values are found in the best *p*-type materials—Zn_4Sb_3, TAGS $[(AgSbTe_2)_{0.15}(GeTe)_{0.85}]$, and $Yb_{14}MnSb_{11}$, all have κ_l values less than 0.5 W/mK. In contrast, many state of the art *n*-type thermoelectric materials exhibit quite high lattice thermal conductivities, as shown in Fig. 7.

Such low κ_l values have been the subject of much discussion for $Ba_8Ga_{16}Ge_{30}$ and other clathrate systems [$Ba_8Al_{14}Si_{32-x}$ has a similar dip at 1000 K, with a minimum κ_l of 0.3 W/mK (Ref. 9)]. Both the rattler atoms in the cage structure[33] and the alloyed host structure[34] significantly reduce the lattice thermal conductivity. The effect of Ga content on lattice thermal conductivity has been studied for $Ba_8Ga_xGe_{46-x}$, with x ranging from 0 to 16.[29] Differences in κ_l between isostructural clathrates likely depend on the electronic environment surrounding the rattler atom.[22] The role of defects and vacancies in altering this local electronic environment has recently been explored.[35,36] Additionally, phonon-charge carrier interactions play a role in reducing κ_l.[14,37]

Figure of merit

These temperature-dependent measurements of Seebeck coefficient (α), electrical resistivity (ρ), and thermal conductivity (κ) permit the calculation of zT ($\alpha^2T/\rho\kappa$) for both the single crystal and polycrystalline material. Figure 8 shows zT increasing with temperature up to 1000 K, where maximum values of 0.80 (single crystal) and 0.74 (polycrystalline) are obtained. While this is significantly lower than the zT of 1.35 reported by Saramat *et al.*, it is similar to the values reported by Kuznetsov *et al.* (0.7, single crystal) and Anno (x=16: 0.65; x=15: 1.0, polycrystalline).[11–13] The difference in zT between our materials and the crystal grown by Saramat *et al.* is largely due to the difference in stoichiometry leading to a smaller Seebeck coefficient but could also be due to measurement uncertainty. In general, estimation of zT requires four distinct measurements which each have a sizable uncertainty, leading to a total uncertainty which may be expressed as $\frac{\Delta z}{z}=2\frac{\Delta\alpha}{\alpha}+\frac{\Delta\sigma}{\sigma}+\frac{\Delta C_p}{C_p}+\frac{\Delta D}{D}$. As the uncertainty in each of these measurements at high temperatures is frequently as large as 10%–20%, the total uncertainty on zT can approach 50%.

When C_p is measured directly, the corrections to zT due to κ and ρ cancel. In our measurements, the corrections for coefficient of thermal expansion in the resistivity $(1+\Delta l/l)$ and thermal conductivity values also provides a comparatively minor decrease (3%) in the zT values we have obtained $(1-2\Delta l/l)$.

Segmentation with other materials

To achieve high efficiency in a real power generation device, a large temperature gradient would be employed with

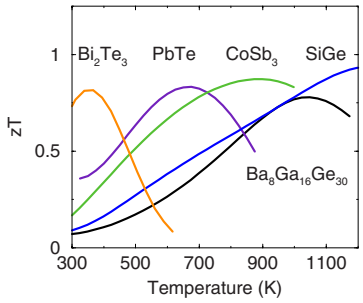

FIG. 8. (Color online) Thermoelectric efficiency (zT) of single crystalline $Ba_8Ga_{16}Ge_{30}$ plotted with other *n*-type high efficiency thermoelectric materials

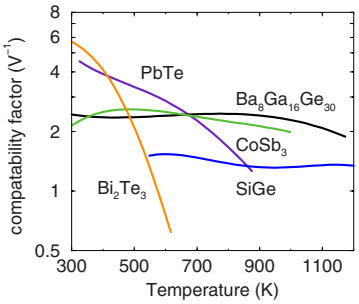

FIG. 9. (Color online) The thermoelectric compatibility factor of several *n*-type thermoelectric materials. Good compatibility arises when the difference is less than a factor of 2. $Ba_8Ga_{16}Ge_{30}$ and $CoSb_3$ show comparable compatibility factors with their adjacent *n*-type materials while SiGe is incompatible.

$Ba_8Ga_{16}Ge_{30}$ segmented with other materials. In a segmented thermoelectric generator, the efficiency depends on more than just the material zT the thermoelectric compatibility must also be considered.[38]

In a thermoelectric device, there is an optimum operation condition which is a compromise between useful thermoelectric effects and Joule heating. Power generation and cooling scale linearly with the current flow, while the Joule heating increases with the square of the current. Because the optimal current density depends on the temperature gradient, it is the reduced variable, relative current density u (V^{-1}) that is important [Eq. (9), where J is the electric current density and $\kappa \nabla T$ is the heat flux].[38,39]

$$u = \frac{J}{\kappa \nabla T}. \tag{9}$$

It can be shown that a material has an optimum efficiency when the relative current density is equal to the thermoelectric compatibility factor s (V^{-1}).[40]

$$s = \frac{\sqrt{1+zT}-1}{\alpha T}. \tag{10}$$

As properties change with temperature, this thermoelectric compatibility factor s varies (Fig. 9). Likewise, between different materials, the value of s will change discontinuously. When the difference in s is greater than about a factor of 2, the actual device efficiency is significantly decreased. As seen in Fig. 9, the compatibility factor of $Ba_8Ga_{16}Ge_{30}$ is similar to the skutterudites ($CoSb_3$-based materials). Both of these materials show good compatibility with their lower temperature neighbor, PbTe. The self-compatibility (flatness of the s vs T line) of $Ba_8Ga_{16}Ge_{30}$ is also quite good, suggesting that its efficiency will not be reduced across a large temperature gradient. The compatibility factor is particularly relevant when segmenting with SiGe: despite a $zT \sim 1$ at high temperatures, the large difference in compatibility factor of SiGe with other materials renders it a poor material for segmentation.

Given the compatibility factors (s) of a segmented leg, the relative current density across a leg (u) may be optimized (Fig. 10). Temperature regions where s and u are dissimilar

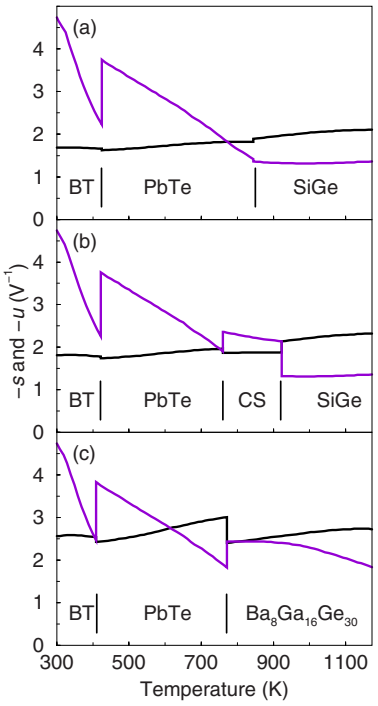

FIG. 10. (Color online) The compatibility factor s (purple) varies between materials and across temperatures. Optimizing the reduced current density u (black) for the maximum efficiency (maximized when $u=s$) results in a compromise. Three legs are shown, based on Bi_2Te_3 (BT), PbTe, SiGe, $CoSb_3$ (CS), and $Ba_8Ga_{16}Ge_{30}$. The two lines are closer in $Ba_8Ga_{16}Ge_{30}$, explaining why its actual efficiency is closer to the maximum efficiency (Fig. 11).

correspond to regions of lower efficiency, while at points where $u=s$ the actual efficiency is equal to the maximum efficiency. Panel (a) corresponds to a leg segmented with Bi_2Te_3, PbTe, and SiGe, (b) Bi_2Te_3, PbTe, $CoSb_3$, and SiGe, and (c) Bi_2Te_3, PbTe, and $Ba_8Ga_{16}Ge_{30}$ across a temperature range of 300–1173 K. Thus, from these curves alone, it is clear that the actual efficiency in a segmented device will be significantly lower than the maximum efficiency. Here, we have have limited the maximum operating temperature for Bi_2Te_3 (600 K), PbTe (875 K), TAGS (775 K), and $CoSb_3$ (1000 K) due to high temperature instabilities. Property values for the skutterudites were obtained from optimized samples measured with the same instruments at the Jet Propulsion Laboratory. While higher zT values have been reported for the skutterudites,[41] the curve shown in Fig. 8 conservatively represents the state of the art.

For small temperature drops, the current density may be maximized (set to s) as the material has no internal compatibility differences. In such a case, Eq. (11) may be used to describe the maximum reduced efficiency.[39] The maximum reduced efficiency (η_r) is shown as the upper line in each panel of Fig. 11. Across large temperature drops, Eq. (12) can be used to calculate the overall maximum efficiency of a single leg.[39] We have done this for three segmented *n*-type legs based on commercially available state-of-the-art materials across 300–1173 K.

$$\max\ \eta_r = \frac{\sqrt{1+zT}-1}{\sqrt{1+zT}+1}, \tag{11}$$

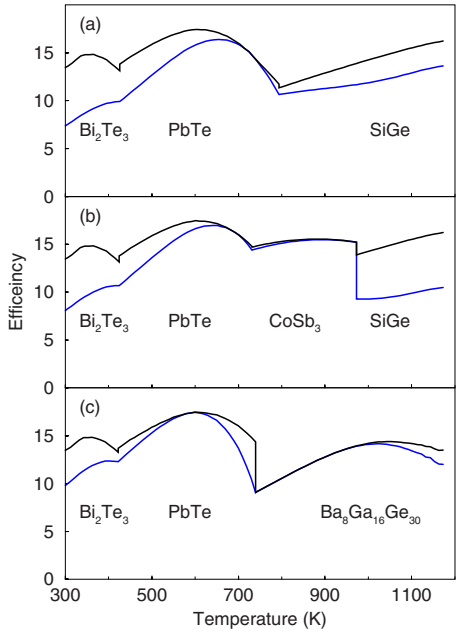

FIG. 11. (Color online) Three segmented thermoelectric leg configurations are considered across a temperature range of 300–1173 K. For each of these, a maximum reduced efficiency (η_{max}) is shown in black and below, shown in blue, is the actual reduced efficiency due to the differences in the compatibility factor.

$$\eta = 1 - \exp\left[-\int_{T_c}^{T_h} \frac{\eta_r}{T} dT\right]. \tag{12}$$

Maximizing the efficiency requires a compromise in relative current density, leading to an actual reduced efficiency given in Eq. (13). Determining the actual efficiency across a large temperature drop again requires the use of Eq. (12).[39] The actual efficiency is shown as the lower blue curve in each panel of Fig. 11. Temperature regions in Fig. 10 where there are large difference between u and s correspond to regions in Fig. 11 with actual efficiencies far below that expected from the material zT.

$$\text{actual } \eta_r = \frac{u(\alpha - u\rho\kappa)}{u\alpha + \frac{1}{T}}. \tag{13}$$

Here, we consider two temperature ranges for thermoelectric power generation: room temperature (300 K) to the maximum working temperature of the skutterudites (923 K) and the clathrates (1173 K). The maximum leg efficiency values for these segmented legs are given in Table II, calculated using Eqs. (11) and (12). Following the method outlined in Ref. 39, actual leg efficiencies are calculated using Eqs. (12) and (13) (Table II).[39] Model thermoelectric devices were simulated with p-type legs of Bi_2Te_3-TAGS-$CeFe_3CoSb_{12}$-$Yb_{14}MnSb_{11}$ (actual leg efficiency of 17.6% across 300–1173 K). Table II lists the resulting device efficiency one could obtain with this p-type leg and the three n-type legs considered. These efficiencies may be used with Eq. (14) [$\bar{T}=(T_h-T_c)/2$] to calculate an effective device ZT (Table II). For T_{hot} of 923 K, the skutterudite-based leg has the highest efficiency, but moving above this temperature requires segmentation with SiGe. At 1173 K, the $Ba_8Ga_{16}Ge_{30}$-based leg shows the highest efficiency despite having a lower material zT and lower max η values for $Ba_8Ga_{16}Ge_{30}$. Thus, zT remains a rough guide for material selection, but in a segmented device, modeling that includes the effect of compatibility is required to compare the actual reduced efficiency.

TABLE II. Comparison of three n-type legs based on Bi_2Te_3–PbTe and a high temperature material (SiGe, $CoSb_3$, or $Ba_8Ga_{16}Ge_{30}$). Legs are modeled across temperature gradients of 300–923 or 1173 K. Modeling predicts a maximum and actual efficiency for each leg, as well as the total efficiency expected for integration with a p-type segmented leg. Device ZT values are extracted from Eq. (14).

Segmented generator efficiency (η)			
923 K	SiGe	$CoSb_3$	$Ba_8Ga_{16}Ge_{30}$
Max. leg η	13.1%	13.6%	13.2%
Actual leg η	11.5%	12.9%	12.4%
Device η	12.9%	13.9%	13.6%
Effective ZT	0.72	0.80	0.77
1173 K	SiGe	$CoSb_3$-SiGe	$Ba_8Ga_{16}Ge_{30}$
Max. leg η	16.2%	16.6%	15.9%
Actual leg η	13.7%	14.2%	15.2%
Device η	15.3%	15.5%	16.4%
Effective ZT	0.75	0.78	0.83

$$\eta_{dev} = \frac{\Delta\bar{T}}{T_h} \frac{\sqrt{1+Z\bar{T}}-1}{\sqrt{1+Z\bar{T}}+T_c/T_h}. \tag{14}$$

CONCLUSION

The thermoelectric properties of single crystalline and polycrystalline $Ba_8Ga_{16}Ge_{30}$ have been investigated in the light of recent reports of high thermoelectric figure of merit (zT) in this n-type material. The extremely low lattice thermal conductivity in this material (minimum of 0.14 W/mK at 1000 K) is comparable to that of a glass. The Seebeck coefficient and electrical resistivitiy generally follow the trend expected from a heavily doped semiconductor where the carrier concentration can be adjusted with the Ga/Ge ratio. While the maximum zT we observe is less than that previously reported, efficiency calculations show that the high thermal stability and good compatibility of

$Ba_8Ga_{16}Ge_{30}$ with other materials still makes it one of the best mid to high temperature *n*-type thermoelectrics. The similar zT values obtained between the polycrystalline and single crystalline materials are particularly promising for commercial applications of $Ba_8Ga_{16}Ge_{30}$.

ACKNOWLEDGMENTS

We thank JPL-NASA, the Danish Research Council, and the Beckman Institute at Caltech for funding and V. A. Ravi for assistance with dilatometry measurements.

*Corresponding author.

[1] G. A. Slack, in *CRC Handbook of Thermoelectrics*, edited by M. Rowe (CRC, Boca Raton, FL, 1995), p. 407.
[2] E. S. Toberer and G. J. Snyder, Nat. Mater. **7**, 105 (2008).
[3] G. J. Snyder, M. Christensen, E. Nishibori, T. Caillat, and B. B. Iversen, Nat. Mater. **3**, 458 (2004).
[4] I. Terasaki, Y. Sasago, and K. Uchinokura, Phys. Rev. B **56**, R12685 (1997).
[5] F. Gascoin, S. Ottensmann, D. Stark, S. M. Haile, and G. J. Snyder, Adv. Funct. Mater. **15**, 1860 (2005).
[6] B. C. Sales, D. Mandrus, and R. K. Williams, Science **272**, 1325 (1996).
[7] G. S. Nolas, J. L. Cohn, G. A. Slack, and S. B. Schujman, Appl. Phys. Lett. **73**, 178 (1998).
[8] B. C. Sales, B. C. Chakoumakos, R. Jin, J. R. Thompson, and D. Mandrus, Phys. Rev. B **63**, 245113 (2001).
[9] C. L. Condron, S. M. Kauzlarich, F. Gascoin, and G. J. Snyder, Chem. Mater. **18**, 4939 (2006).
[10] L. Bertini, K. Billquist, D. Bryan, M. Christensen, C. Gatti *et al.*, 22nd International Conference on Thermoelectrics, p. 127, 2003.
[11] V. L. Kuznetsov, L. A. Kuznetsova, A. E. Kaliazin, and D. M. Rowe, J. Appl. Phys. **87**, 7871 (2000).
[12] A. Saramat, G. Svensson, A. E. C. Palmqvist, C. Stiewe, E. Mueller, D. Platzek, S. G. K. Williams, and D. M. Rowe, J. Appl. Phys. **99**, 023708 (2006).
[13] H. Anno, M. Hokazono, M. Kawamura, J. Nagao, and K. Matsubara, 21st International Conference on Thermoelectrics, p. 77, 2002.
[14] A. Bentien, M. Christensen, J. D. Bryan, A. Sanchez, S. Paschen, F. Steglich, G. D. Stucky, and B. B. Iversen Phys. Rev. B **69**, 045107 (2004).
[15] J. L. Cohn, G. S. Nolas, V. Fessatidis, T. H. Metcalf, and G. A. Slack, Phys. Rev. Lett. **82**, 779 (1999).
[16] B. C. Sales, D. G. Mandrus, and B. C. Chakoumakos, in *Recent Trends in Thermoelectric Materials Research II*, edited by T. Tritt (Academic Press, San Diego, 2001), pp. 1–36.
[17] V. Keppens, B. C. Sales, D. Mandrus, B. C. Chakoumakos, and C. Laermans, Philos. Mag. Lett. **80**, 807 (2000).
[18] J. A. McCormack and J. P. Fleurial, in *Modern Perspectives on Thermoelectrics and Related Materials*, edited by D. D. Allred, C. R. Vining, and G. A. Slack, MRS Symposia Proceedings No. 234 (Materials Research Society, Pittsburgh, 1991), p. 135.
[19] C. Wood, D. Zoltan, and G. Stapfer, Rev. Sci. Instrum. **56**, 719 (1985).
[20] A. T. Burkov and M. V. Vedernikov, in *Condensed Matter. Disordered Solids*, edited by S. K. Srivastava and N. H. March (World Scientific, Singapore, 1995), Chap. 6, p. 361.
[21] A. Bentien, E. Nishibori, S. Paschen, and B. B. Iversen, Phys. Rev. B **71**, 144107 (2005).
[22] M. Christensen, N. Lock, J. Overgaard, and B. B. Iversen, J. Am. Chem. Soc. **128**, 15657 (2006).
[23] D. M. Rowe and G. Min, J. Mater. Sci. **14**, 617 (1995).
[24] H. J. Goldsmid and J. W. Sharp, J. Electron. Mater. **28**, 869 (1999).
[25] G. K. H. Madsen, K. Schwarz, P. Blaha, and D. J. Singh, Phys. Rev. B **68**, 125212 (2003).
[26] M. Cutler, J. F. Leavy, and R. L. Fitzpatrick, Phys. Rev. **133**, A1143 (1964).
[27] T. Amano, B. J. Beaudry, K. A. Gschneidner, Jr., R. Hartman, C. B. Vining, and C. A. Alexander, J. Appl. Phys. **62**, 819 (1987).
[28] Heat capacity values used in Ref. 12 were constant above 700 K with a value of 0.30 J/g K; A. Saramat (private communication).
[29] N. L. Okamoto, K. Kishida, K. Tanaka, and H. Inui, J. Appl. Phys. **100**, 073504 (2006).
[30] N. L. Okamoto, K. Kishida, K. Tanaka, and H. Inui, J. Appl. Phys. **101**, 113525 (2007).
[31] H. J. Goldsmid, in *Applications of Thermoelectricity*, edited by B. L. Worsnop (Methuen and Co., London, 1960).
[32] M. Christensen and B. B. Iversen, Chem. Mater. **19**, 4896 (2007).
[33] M. Christensen, F. Juranyi, and B. B. Iversen, Physica B **385**, 505 (2006).
[34] N. L. Okamoto, J. H. Kim, K. Tanaka, and H. Inui, Acta Mater. **54**, 5519 (2006).
[35] W. Carrillo-Cabrera, S. Budnyk, Y. Prots, and Y. Grin, Z. Anorg. Allg. Chem. **630**, 2267 (2004).
[36] W. Carrillo-Cabrera, R. C. Gil, S. Paschen, and Y. Grin, Z. Kristallogr. **217**, 183 (2002).
[37] A. Bentien, S. Johnsen, and B. B. Iversen, Phys. Rev. B **73**, 094301 (2006).
[38] G. J. Snyder, Appl. Phys. Lett. **84**, 2436 (2004).
[39] G. J. Snyder, in *Thermoelectrics Handbook Macro to Nano*, edited by D. M. Rowe (CRC, Boca Raton, FL, 2006), pp. 1–9.
[40] G. J. Snyder and T. S. Ursell, Phys. Rev. Lett. **91**, 148301 (2003).
[41] L. D. Chen, T. Kawahara, X. F. Tang, T. Goto, T. Hirai, J. S. Dyck, W. Chen, and C. Uher, J. Appl. Phys. **90**, 1864 (2001).